# An Ab Initio-Derived Force Field for Amorphous Silica Interfaces for Use in Molecular Dynamics Simulations

Hasini S. Senanayake,<sup>†</sup> Pubudu N. Wimalasiri,<sup>†</sup> Sahan M. Godahewa,<sup>†</sup> Ward H. Thompson,<sup>\*,†</sup> and Jeffery A. Greathouse<sup>\*,‡</sup>

†Department of Chemistry, University of Kansas, Lawrence, KS 66045, USA ‡Nuclear Waste Disposal Research & Analysis Department, Sandia National Laboratories, Albuquerque, New Mexico 87185, USA

E-mail: wthompson@ku.edu; jagreat@sandia.gov

### Abstract

We present a classical interatomic force field, silica-DDEC, to describe the interactions of amorphous and crystalline silica surfaces, parametrized using density functional theorybased charges. Charge schemes for silica surfaces were developed using the Density Derived Electrostatic and Chemical (DDEC) method, which reproduces atomic charges of the periodic models as well as the electrostatic potential away from the atom sites. Lennard-Jones parameters were determined by requiring the correct description of i) the amorphous silica density, coordination defects, and local coordination geometry, relative to experimental measurements, and ii) water-silica interatomic distances compared to ab initio results. Deprotonated surface silanol sites are also described within the model based on DDEC charges. The result is a general electronic structure-derived model for describing fully flexible amorphous and crystalline silica surfaces, and interactions of liquids with silica surfaces of varying structure and protonation state.

### 1 Introduction

Silica is the most abundant metal oxide and one of the main constituents of the Earth's crust.

Nanoscale silica structures are ubiquitous in geologic materials such as sedimentary rocks, zeolites, and clay minerals and are therefore important in a wide variety of geological applications, including subsurface transport of aqueous solutions and complex fluids (e.g.,  $CO_2$ , oil, and gas) and nuclear waste disposal. Nanoconfinement particularly affects the stability of mineral phases, mineral-water interface chemistry, fluid migration and transport, as well as reaction kinetics. 1-5 Silica surface interactions with water and other fluids can be productively probed by combining microscopic and spectroscopic studies. 6,7 However, the molecular-level details of the aqueous silica interface are still elusive because of limits in experimental spatial and temporal resolution. Thus, molecular dynamics (MD) simulations are a critical complementary tool in providing a detailed understanding of structural and dynamical properties of silicaliquid interfaces.

Underlying these simulations are the descriptions of the interactions, which ultimately determine their ability to describe the system. Approaches have included density functional theory (DFT)<sup>8–16</sup> as well as classical reactive<sup>17–21</sup> and fixed-charge force fields. <sup>22–31</sup> Each has their own limitations and advantages, but improvement is still needed in each. In the present work, we focus on the latter category

(which is particularly useful for describing large systems and long timescales) and use DFT calculations to determine the correct electrostatic interactions of silica. Specifically, we use Density Derived Electrostatic and Chemical <sup>32,33</sup> (DDEC) net atomic charges <sup>34</sup> (NACs) generated from periodic electronic structure calculations to determine atomic charges that reflect the electrostatic environment of bulk and slab models, as well as the electrostatic potential at interfaces. The force field is then completed by the addition of Lennard-Jones (LJ) interactions to represent the shorter-ranged dispersion effects.

Many interatomic potentials have been developed to reproduce the structural and mechanical properties of silica; see for example the Supporting Information of Emami et al.<sup>31</sup> for a review. Interaction parameters have been based on general force fields such as Clayff, <sup>23</sup> the van Beest, Kramer, and van Santen (BKS) potential, <sup>35</sup> and CVFF <sup>36</sup> or, alternatively, derived based on microscopic (e.g., surface energies and geometries <sup>31</sup>) or macroscopic (e.g., wetting and mechanical behavior <sup>31,37</sup>) properties. Ab initio calculations offer an important route to improve force fields by direct determination of some of the parameters.

Most of the silica force fields were designed to properly describe the structural properties and phase behavior of silica rather than the interactions of silica with liquids, including water. Given the central role of silica/water interfaces in geochemistry, separations, and other applications, it is critical to develop force fields that accurately describe the interfacial properties with a fully flexible model, 30 i.e., one in which the silica structure does not need to be held fixed. Moreover, the majority of force fields are implemented for neutral silica therefore these parameters are applicable only for silica-water interfaces at lower pH. When in contact with aqueous solutions at higher pH, deprotonation of silanols can take place, leading to negatively charged surfaces. 31 Hence force fields are needed that can describe these charged surfaces realistically, but this has received relatively little attention. <sup>27,30</sup>

The BKS potential<sup>35</sup> is perhaps the most

widely used to simulate crystalline as well as amorphous silica.  $^{38-41}$  This force field is based on a mixed approach in which *ab initio* cluster models and empirical  $\alpha$ -quartz crystallographic data are combined to determine the parameters to obtain a force field capable of describing multiple silica polymorphs.

The charges on the silica atoms, particularly those at surface sites, are central in determining the behavior of a liquid at the silica interface. This provides a strong impetus to accurately model these charges to best reflect the electrostatic potential near the surface. Therefore, in this paper, we parameterize silica charges using the DDEC analysis based on the NACs. This method is designed to accurately describe the electrostatic potential presented by the system outside of its electron distribution. A key feature of the DDEC method is its ability to produce chemically meaningful NACs when applied to periodic materials. The method combines two atoms-in-molecule approaches namely, iterative Hirshfeld and iterated Stockholder atoms, to partition the total electron density among atoms and uses a distributed multipole expansion to reproduce the electrostatic potential outside the electron distribution. This method has been successfully used for force field development 42-45 and to our knowledge this is the first time it has been used to calculate the NACs of amorphous silica surfaces to generate a force field. In addition, the DDEC approach provides key insight on the extent of charge redistribution around the negatively charged oxygen atoms produced by loss of a proton for silica at higher pH.

The remainder of this paper is organized as follows. After a description of the computational methods, we present the results obtained for DDEC net atomic charges for both crystalline and amorphous silica bulk as well as neutral and deprotonated surfaces. We then describe the selection of LJ parameters through a broad search in parameter space. Finally, we present a characterization of the structural and defect properties of silica obtained with molecular dynamics simulations to validate the force field.

### 2 Computational details

## 2.1 Density Derived Electrostatic and Chemical Calculations

All DFT calculations were carried out with version 5.4.4 of the Vienna ab initio Simulation Package (VASP). 46-48 As discussed below, both bulk and slab geometries of crystalline (cristobalite) and amorphous silica models were con-The general approach used an orthorhombic supercell of silica with the z-axis perpendicular to the basal (0001) plane of the hexagonal unit cell periodically repeated in the three Cartesian directions for the bulk silica systems (the cell dimensions are given in the Supporting Information). The lattice vectors were set to box dimensions to create a regular mesh centered at  $\Gamma = 0$ . In the case of slab systems, the only difference was that a  $\sim 20$  Å thick vacuum region was inserted in the z-direction. A plane wave basis set with a projector augmented wave (PAW) pseudopotential and Perdew-Burke-Ernezhof (PBE) functional was used in all calculations with an energy cutoff of 400 eV. The geometry of each system was optimized using the conjugate gradient method.

### 2.2 Classical MD Generation of Silica Structures

All MD simulations were performed using the LAMMPS code. <sup>49</sup> Bulk and slab amorphous silica models used in this work were generated using a melt-cleave-quench procedure. 41 Briefly, a bulk amorphous silica structure is heated to 3000 K over 1 ns to form molten silica; this step is performed in the NPT (fixed number, pressure, and temperature) ensemble. Then, the periodic simulation cell is expanded in the zdirection to 80 Å, cleaving the molten silica to generate a slab with a surface normal to the z-direction. The resulting slab is then equilibrated at 3000 K for 1 ns in an  $NP_zAT$  ensemble where  $P_z$  is the pressure in z (1 atm) and A is the xy surface area; for bulk silica models, the cleaving step is omitted. During this step, atomistically different models were obtained by using different initial velocities selected from a Boltzmann distribution. Then these systems were cooled at a rate of 1 K/ps by ramping down the temperature in the same  $NP_zAT$  ensemble to generate amorphous silica surfaces at 298 K. In all simulations temperature and pressure were maintained by a Berendsen thermostat <sup>50</sup> (damping constant of 1 ps) and a Berendsen barostat <sup>50</sup> at 1.0 atm (time constant of 1 ps, modulus parameter of 360,000 atm), respectively. The long-range electrostatic interactions were included using three-dimensional periodic boundary conditions and the particle-particle particle-mesh (PPPM) solver with a tolerance of  $10^{-4}$  and a cutoff of 9.5 Å.

The amorphous slab models were functionalized by an ad hoc procedure. First, surface hydroxyls representative of dissociative water adsorption were created by adding an H atom to a singly coordinated O and an OH group to a three-coordinate Si atom. Overlap with other surface atoms is avoided to prevent unrealistic surface defects and to minimize coordination defects in the slabs. This process was repeated until no pairs of 1-coordinate O and 3-coordinate Si atoms remained. Second, the strained two-membered (2M) and threemembered (3M) rings on the surface were functionalized by addition of water to the Si-O-Si moiety closest to the slab surface to generate vicinal silanols. A ring is defined as a cycle of Si-O bonds with a given number of Si atoms, e.g., 2M rings have two Si atoms and 3M rings have three Si atoms. The ring identification procedure is discussed in detail in our previous paper. 41 Finally, the slab silanol groups were relaxed (using force-field parameters in Table 2) for 1 ns at 298 K in the same  $NP_zAT$  ensemble.

For comparison, amorphous silica bulk and slab systems were generated using the BKS, ClayFF,  $^{51}$  Takada,  $^{52}$  Carré, Horbach, Ispas, Kob (CHIK),  $^{53}$  SHIK-1,  $^{54}$  and SHIK-2,  $^{54}$  force fields with the same procedure, with one exception. To generate molten silica, the  $\beta$ -cristobalite structure was heated up to 8000 K for BKS, but up to 4000 K for the other force fields. The details of these force fields are given in the Supporting Information. The structural features, including coordination defects and ring distributions, generated with each of

these force fields were used for comparison with the new silica-DDEC force field.

In order to gain a first understanding of how the force field describes silica-water interactions, a slit pore model was formed by placing a slab of liquid water of size  $\sim 30$  Å between two silica surfaces of dimension  $21.0155 \text{ Å} \times 21.0155 \text{ Å}$ . Both neutral and deprotonated (charge density of 0.3 charges/nm<sup>2</sup>) slabs were used. The SPC/E model<sup>55</sup> was used to describe the water molecules. The systems were equilibrated in the  $NP_zAT$  ensemble for 2 ns, allowing the silica atoms to move, with only the silanol Si-O (or Si-O<sup>-</sup>) and O-H bonds and Si-O-H angle held fixed using SHAKE. 56 The long-range electrostatic interactions were included using three-dimensional periodic boundary conditions and the particleparticle particle-mesh (PPPM) solver with a tolerance of  $10^{-4}$  and a cutoff of 10.5 Å. The slit pore simulation was run for additional 4 ns in the NVT ensemble and the configurations were saved every 100 fs in the final 2 ns of the NVT simulation to calculate the probability distributions for silica-water distances.

# 3 Determination of the force field

Force field parameters were developed in the following order. First, the atomic charges were determined from the DDEC analysis. Second, the non-bonded Lennard-Jones interactions were obtained by requiring amorphous silica structural properties to be consistent with experiment. Third, the intramolecular potentials for silanols were adopted from existing force fields. Fourth, minor adjustments to the silica-water LJ parameters were made based on simulations of the interface.

# 3.1 Neutral Surface Atomic Charges

#### 3.1.1 DDEC Analysis

The DDEC method was used to determine the atomic charges in order to accurately describe

the electrostatic potential that liquid (or gas) molecules will encounter at a silica interface. In order to determine charges that are general for neutral silica, we considered four different systems, which are illustrated in Fig. 1: a) Bulk  $\beta$ -cristobalite, b) Bulk amorphous silica (five separate structures), c) A  $\beta$ -cristobalite slab, and d) Amorphous silica slabs (five structures). The system parameters are given in the Supporting Information. The silanol density on the surface of each slab model is  $\sim 4 \text{ OH/nm}^2$ . The amorphous silica models were taken from those generated in a previous study<sup>41</sup> based on the BKS model, while bulk cristobalite structures were built in the Visual Molecular Dyanmics (VMD)<sup>57</sup> inorganic builder and slab cristobalite structures were taken from the literature. <sup>58</sup> The geometry of each system was first optimized within the DFT approach described in Sec. 2.1 before a single point energy calculation was carried out for the DDEC analysis.

The DDEC method calculates the charges for each atom in the model individually. Thus, we focus on the average NAC for each equivalent atom type. The charge distributions are shown for the slab models in Figs. S1 and S2 and the charge ranges are shown in Fig. S3. Average charges resulting from these calculations are presented in Table 1. We first discuss the bulk systems shown in Fig. 1a,b. Interestingly, the DDEC analysis finds nearly identical average charges for the  $\beta$ -cristobalite and amorphous silica systems with  $q_{Si} = 1.87$  and  $q_O = -0.93$ , as shown in Table 1 (all charges are in units of the elementary charge e). These charges are consistent with those obtained from DDEC calculations of zeolites. 45 The primary difference between the two is that the amorphous system has a wider distribution of atomic charges due to the greater variation in local environments.

The slab models display slightly modified charges relative to the bulk systems. The average (non-silanol) silicon and oxygen charges are relatively close to the bulk results, within 0.04. In the silanol groups, the charges are shifted to smaller absolute values, with  $q_{Si(OH)} \sim 1.8$  and  $q_O = -0.84$  in amorphous silica and -0.9 in cristobalite. The silanol hydrogen charge is consistent between the two slab mod-

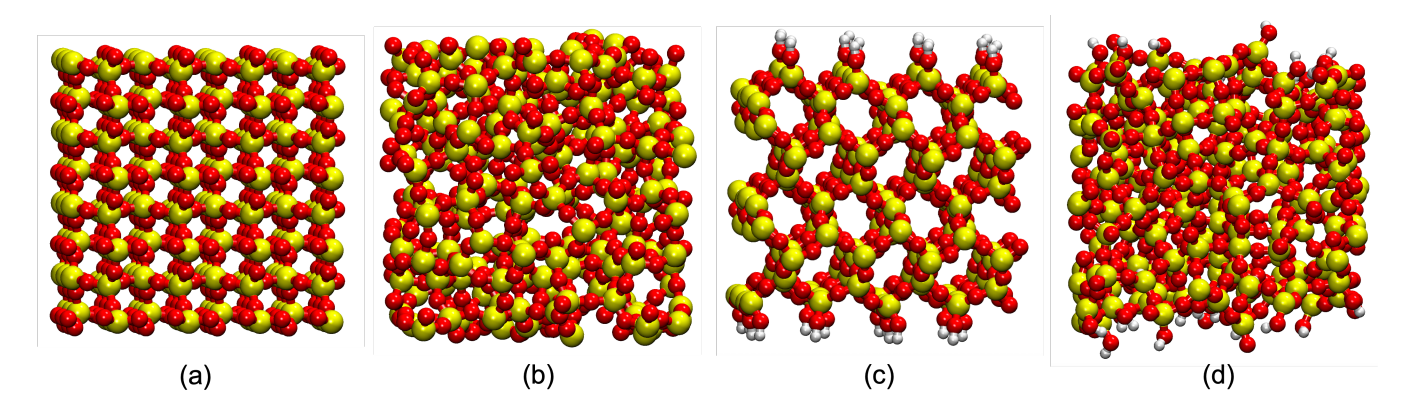


Figure 1: Neutral model silica systems used for the DDEC calculations: (a) Bulk  $\beta$ -cristobalite, (b) Bulk amorphous silica, (c)  $\beta$ -cristobalite slab, and (d) Amorphous silica slab. Five independent models of each of the amorphous silica systems, (b) and (d), were considered. (Si = yellow, O = red, H = white)

Table 1: Average net atomic charges (NAC) in units of the elementary charge e of different atom types in silica obtained from the DDEC analysis. The standard deviation in the value of the trailing digit, obtained from the different models and all equivalent atoms, is shown in parentheses.

Silica system	Si	О	Si(OH)	O(H)	H(O)	$Si(O^{-})$	O-	O(SiO <sup>-</sup> )
crystalline (bulk)	1.868(1)	-0.934(1)	-	-	-	-	-	-
amorphous (bulk)	1.87(3)	-0.93(2)	-	-	-	-	-	-
crystalline (slab)	1.88(1)	-0.94(1)	1.83(1)	-0.85(1)	0.429(2)	-	-	-
amorphous (slab)	1.86(4)	-0.93(3)	1.80(4)	-0.84(3)	0.43(2)	-	-	-
crystalline (slab; deprotonated site)	1.88(1)	-0.94(1)	1.83(2)	-0.85(2)	0.43(1)	1.71(2)	-1.01(1)	-0.92(2)
amorphous (slab; deprotonated site)	1.85(3)	-0.93(2)	1.79(3)	-0.85(3)	0.43(1)	1.73(1)	-0.99(4)	-0.90(2)

els (0.42 - 0.43).

In determining the atomic charges for a force field, we aimed for simplicity. This is enabled by the closely clustered results for the Si and (non-silanol) O atom charges from the DDEC results for the neutral systems. Thus, we choose  $q_{Si} = 1.86$  and  $q_O = -0.93$   $(q_{Si} = 2 * q_O)$ , which are very close to those of the bulk systems and are within 0.03 of every average NAC for the four neutral systems shown in Fig. 1. The same priority for simplicity, along with only modest differences in the average charges, motivates the choice to use the same Si charge for atoms in silanol groups. Finally, the silanol O and H charges are constrained by these choices and the electroneutrality requirement when an Si - O - Si group is functionalized via hydrolysis as  $H_2O + Si - O - Si \rightarrow 2(Si - O - H)$ . The latter gives the silanol oxygen charge as  $q_{O(H)} =$   $(q_O/2) - q_{H(O)}$ . This approach, however, only applies to neutral systems with an even number of silanols. In order to ensure that the charges will also give a locally neutral system, we further require that  $q_{Si}/4 = q_{O(H)} + q_{H(O)}$  based on a bond increment approach that divides the charge on an atom by the number of bonds that it makes. This small adjustment leads to  $q_H = 0.433$ , which gives  $q_{O(H)} = -0.898$ . This charge scheme for fully neutral silica is shown in Fig. 2.

### 3.1.2 Comparison with Previous Charge Schemes

It is interesting to compare these *ab initio*-derived charges to those used in other force fields for silica. The Si charges used in different force fields span a large range, from 0.5 to 4.0.<sup>59</sup> The most widely used model for sil-

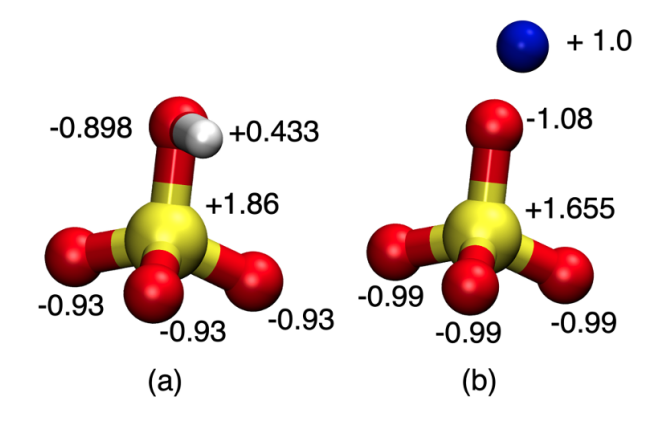


Figure 2: The silica-DDEC charge scheme for (a) neutral silanol sites and bulk silica, and (b) deprotonated silanol sites and the neighboring O atoms. (Si = yellow, O = red, H = white,  $Na^+ = blue$ )

ica structure and phase behavior is the BKS force field.<sup>35</sup> It has significantly larger charges,  $q_{Si} = 2.4$  and  $q_O = -1.2$ , than those obtained here. This is perhaps not surprising given that the goal in its design was the description of bulk crystalline and amorphous silica structure and phase behavior. It has been much less widely used in simulations of silica interfaces, though Hassanali *et al.* have adapted it for this purpose, <sup>26,27</sup> using the BKS charges for silanol silicon and silanol oxygen atoms and thus 0.6 for silanol hydrogens.

On the other hand, Clayff was specifically designed for "layered aluminosilicates and their aqueous interfaces." <sup>23</sup> The Clayff charges are derived from Mulliken and ESP analysis of DFT results. Compared to BKS, they are closer to, but still larger than, those found here, with  $q_{Si} = 2.1$  and  $q_O = -1.05$ . Clayff is capable of describing silanol groups and assumes charges of  $q_{Si(OH)} = 2.1$ ,  $q_{O(H)} = -0.95$ , and  $q_{H(O)} = 0.425$ , so that the silanol oxygen and hydrogen charges are reasonably close to the present values.

One of us has previously developed the Gulmen-Thompson force field <sup>24,25</sup> particularly to describe silica-liquid interactions and widely applied it to problems of liquids confined in silica mesopores, including several properties for which comparisons with experimental results are available for validation. <sup>25,60–63</sup> This descrip-

tion has charges that are significantly smaller in magnitude,  $q_{Si} = 1.28$ ,  $q_O = -0.64$ ,  $q_{O(H)} = -0.74$ , and  $q_{H(O)} = 0.42$ . These charges were adapted from the work of Bródka and Zerda, <sup>22</sup> who obtained their charges from semiempirical electronic structure calculations on silica cluster models.

Tangney and Scandolo used plane-wave DFT calculations to parameterize a bulk silica force field.  $^{64}$  They obtained charges even larger than those of BKS:  $q_{Si} = 2.76514$  and  $q_O = -1.38257$ . However, their force field is polarizable and thus these charges are not directly comparable to the other fixed-charge force fields. Similarly, Pedone *et al.* developed the FFSiOH force field that is based on a partial charge shell-ion model calibrated against DFT simulations.  $^{28}$  The partial charges used in their model are also larger than those found here, but should naturally be viewed in the context of the different modeling approach.

A number of other force fields that have been parameterized by electronic structure calculations make use of explicit bonded terms, i.e., bond stretching and angle bending potentials between bonded atoms. As such, they are aimed at describing pre-determined structures, e.g., they cannot be applied to model the melting of silica and subsequent formation of amorphous silica structures by quenching to the solid. The force field of Heinz and co-workers<sup>31</sup> is a key example of this approach that has been used to model atomistic details of interfacial silica properties. They used charges developed from crystallographic electron densities, which are also much smaller than those found here:  $q_{Si} = 1.1, q_O = -0.55, q_{O(H)} = -0.675, \text{ and}$  $q_{H(O)} = 0.4$ . Much earlier, Hill and Sauer developed force fields for silica<sup>65</sup> and aluminosilicates 66 in much the same spirit. They determined charges based on Hartree-Fock calculations with straightforward population analysis. They used a charge increment approach, which yields comparatively small charges, e.g.,  $q_{Si} = 0.5236.$ 

Butenuth et al. used ab initio (DFT and MP2) calculations with charges estimated from Bader and electrostatic potential analyses for quartz, amorphous silica slabs, and amorphous

silica cluster models.<sup>30</sup> They proposed a charge scheme of  $q_{Si} = 1.6$ ,  $q_O = -0.8$ ,  $q_{O(H)} = -0.8$ , and  $q_{H(O)} = 0.4$ , which is more similar to that of the present work. However, they have defined a single charge for silanol and siloxane oxygens. Interestingly, these Si and O charges are the same as those proposed, based on empirical data, by Vashishta *et al.*<sup>67</sup> in their three-body potential model.

#### 3.1.3 Lennard-Jones Parameters

With the net atomic charges in hand from the DDEC analysis, the next component of the force field is the short-range non-bonded interactions. We adopt a Lennard-Jones (LJ) form for these with the parameters determined by a broad parameter search to identify values that give, in combination with the determined charge scheme: 1) The correct density for amorphous silica, 2) A minimal number of coordination defects, and 3) Accurate description of the local coordination geometry.

To determine the optimum LJ parameters, we carried out a systematic search. Specifically, we examined 4455 different LJ parameter sets, with  $\sigma_{Si}$  varied from 2.0 to 2.8 Å and  $\sigma_O$  from 2.6 to 3.0 Å in increments of 0.1 Å,  $\epsilon_{Si}$  ranging from 0.00004 - 0.0002 kcal/mol in increments of 0.00002 kcal/mol, and  $\epsilon_O$  from 0.4068 to 0.5068 kcal/mol in increments of 0.01 kcal/mol. (Higher values of  $\sigma_{Si}$  or lower values of  $\sigma_O$  were found to yield incorrect densities independent of the  $\epsilon$  values.) For each case the melt-quench procedure was performed to generate a bulk amorphous silica model. The first screening was for the density and coordination defects of the bulk amorphous silica structures at room temperature. Only LJ parameter sets that produced a density between  $2.1 - 2.3 \text{ g/cm}^3$  and gave more than 99.5% of the silicon atoms as four-coordinate were considered further. The density variation with  $\sigma_{Si}$ ,  $\sigma_O$ ,  $\epsilon_{Si}$  and  $\epsilon_O$  during the melt-quench procedure is shown in Figures S4-S7 respectively.

These LJ parameter combinations were used to generate unfunctionalized amorphous silicaslabs using the melt-cleave-quench approach described in Sec. 2.2. The introduction of a silicavacuum interface introduces additional coordination defects. Thus, we considered only LJ parameters that gave more than 99.0% of the silicon atoms as four-coordinate, which left only seven combinations. Among these, three of the LJ parameters occur in relatively narrow ranges, namely  $\sigma_{Si}$  (2.6 – 2.8 Å),  $\sigma_{O}$  (2.7–2.8 Å), and  $\epsilon_{Si}$  (0.0001–0.0002 kcal/mol). The last parameter,  $\epsilon_{O}$ , showed greater variation, with most values falling in the range 0.4568 – 0.4768 kcal/mol, but two cases where  $\epsilon_{O} = 0.4168$  or 0.4068 kcal/mol.

It is likely that all of these seven LJ parameter sets will yield similar behavior for amorphous silica. However, to further refine the selection, we used each set to generate 10 atomistically distinct amorphous silica slabs that were functionalized using the *ad hoc* procedure in Sec. 2.2. (Note that functionalization typically removes some of the surface defects.) We then chose the parameter set, the values for which are given in Table 2, that gave the largest number of functionalized slabs without any defects.

Additional parameters are required to describe surface silanol groups of functionalized slabs. Slab models were functionalized as described in Sec. 2.2, equilibrated for 1 ns in the  $NP_zAT$  ensemble, and trajectories were then propagated for 2 ns in the NVT ensemble. This was repeated for ten slab models for each LJ parameter set and coordination defects were examined every 1 ps within the final 1 ns of the NVT trajectories. For the silanol oxygen,  $\epsilon_{O(H)}$ was taken to be the same as for the oxygen atom in the TIP4P/2005 water model<sup>68</sup> and  $\sigma_{O(H)}$ was varied from 2.9 to 3.5 Å in increments of 0.1 Å. No LJ interactions for the silanol hydrogen were included. The optimum  $\sigma_{O(H)}$ , given in Table 2, was chosen to be the one which gave the largest fraction of four-coordinate silicon in these tests.

It is important to note that the LJ parameters derived here and presented in Table 2 are calibrated to describe amorphous silica structures in coordination with the DDEC-derived charges. These parameters effectively describe the Si-O covalent bond in silica, in contrast to the typical application of a Lennard-Jones model for intermolecular interactions. This

Table 2: The proposed silica-DDEC force field charges and Lennard-Jones parameters. Lorentz-Berthelot mixing rules were used to calculate  $\sigma_{i,j}$  and  $\epsilon_{i,j}$  where  $i \neq j$ .

	Atom type	q(e)	σ (Å)	$\epsilon \; (\mathrm{kcal/mol})$	
Framework Sites	$\mathrm{Si}^a$	1.86	2.7	0.0001	
	$\mathrm{Si}^b$	1.86	3.0	0.01	
	$O^a$	-0.93	2.7	0.4668	
	$O_p$	-0.93	3.3	0.1852	
Silanols	O(H)	-0.898	3.3	0.1852	
	H(O)	0.433	0.0	0.0	
Deprotonated Sites	$Si(O^{-})$	1.655	2.7	0.0001	
	O-	-1.08	3.3	0.1852	
	$O(SiO^{-})$	-0.99	2.7	0.4668	

<sup>&</sup>lt;sup>a</sup>In interactions with other silica atoms

can be seen, for example, in the unusually small value of  $\sigma_O$ . The DDEC charges describe the electrostatic potential external to the silica atoms, but the LJ parameters are not designed to describe interactions of external molecules with the surface. This is addressed in Sec. 4.4 by simulation of the silica-water interface. The results show that it is sufficient to modify the LJ parameters between the silica oxygen sites with molecules in contact with the surface in a simple way; this is reflected in Table 2. Note that this means that the silica-DDEC force field forsakes typical combination rules, and instead uses different LJ parameters for interactions within the silica and for interactions with molecules external to the silica.

### 3.1.4 Silanol and Geminal Intramolecular Potentials

Bonded terms are also included between the atoms in silanol groups in the form of harmonic potentials for bond stretching and angle bending, which were taken from the Gulmen-Thompson force field <sup>24,25</sup> (see Table S1). Often in simulations we constrain the Si-O and OH bond distances and Si-O-H angles for the silanols, but the harmonic potentials given in Table S1 can also be used with little change in behavior of the silica surface. Torsion po-

tentials have not been used due to the limited number of rotational degrees of freedom in these systems.<sup>31</sup>

# 3.2 Deprotonated Surface Atomic Charges

We next consider the charges associated with a deprotonated silanol site, which is essential for describing silica in aqueous solutions at pH greater than the isoelectric point.

#### 3.2.1 DDEC Analysis

To investigate the charges around a deprotonated silanol group we considered five cristobalite slabs (that differ in the location of a single deprotonated site) and five amorphous silica slabs with a single deprotonated silanol. To make the systems charge neutral a Na<sup>+</sup> ion and six solvating water molecules were added to the simulation cell away from each surface as shown in Fig. 3. The VASP inputs for each system is included in the Supporting Information.

The DDEC net atomic charges for the surfaces with a single deprotonated site are given in Table 1. The charges shown are averages over all the atoms of the same type within each slab and over the multiple slab models. To preserve the simplicity of the force field,

<sup>&</sup>lt;sup>b</sup>In interactions with water molecules

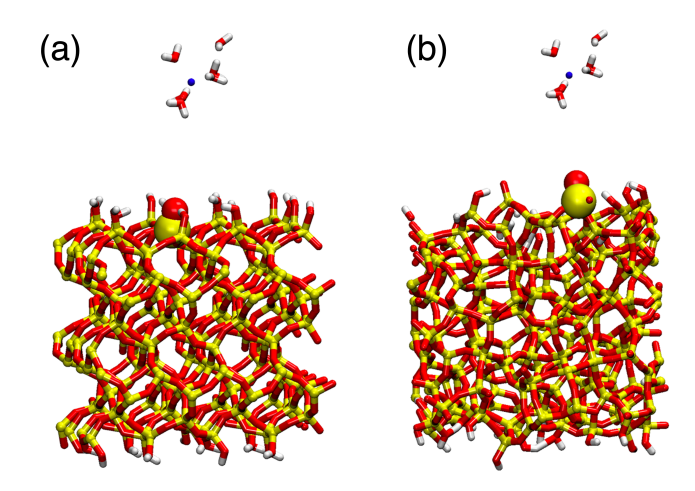


Figure 3: Deprotonated (a) cristobalite and (b) amorphous silica surfaces with one deprotonated site each, indicated by the larger spheres. A sodium ion (blue) with six solvating water molecules was added, away from the surface, to make the system overall charge neutral.

and because silica is an insulator, we consider only local charge changes around the deprotonation site, specifically, the central Si-O<sup>-</sup> moiety and the three bridging oxygens bound to that silicon atom. The DDEC calculations indicate that charge redistribution upon deprotonation is primarily limited to the O<sub>3</sub>Si-O<sup>-</sup> site, and that nearby atoms have charges that are not significantly distinguishable from those averaged over the rest of the slab. Indeed, we see that the DDEC charges of the silica framework and other silanols are very similar to those for the slabs with no deprotonated silanol (see Table 1).

The essential feature of the DDEC charge shifts upon deprotonation are 1) the Si charge becomes more negative by  $\sim -0.15$ , 2) the silanol oxygen that loses a proton becomes more negative by  $\sim -0.1$ , and 3) the charges of the three O atoms attached to the central silicon become more negative by  $\sim -0.06$ . However, these charge shifts are not sufficient in magnitude to describe the full negative charge remaining on the slab, due to some delocalization of the charge over the entire system within the DFT description. We have thus chosen charges that reproduce these essential features while maintaining a local charge redistribution. Thus, the charges, shown in Table 2 and Fig. 2,

have a reduced silicon charge of  $q_{Si(O^-)} = 1.655$  and a more negative terminal oxygen,  $q_{O^-} = -1.08$ ; the charges on the three oxygens bound to the Si are then chosen to complete the full negative charge on the slab,  $q_{O(SiO^-)} = -0.99$ , while preserving the charge difference with the terminal  $O^-$  found in the DDEC calculations.

### 3.2.2 Comparison with Previous Charge Schemes

Models that include a description of deprotonated silanols range from nearly complete localization of the negative charge <sup>27,30,31</sup> to complete delocalization of the charge. <sup>69</sup> A number of groups have used a localized redistribution of charge to describe dissociated silanol groups. Hassanali *et al.* changed only the oxygen charge upon silanol deprotonation in their models based on the BKS force field for silica. <sup>26,27</sup>

Butenuth et al. used ab initio calculations with electrostatic potential-based charges on quartz, amorphous silica slabs, and amorphous silica cluster models. 30 They also found that such charge analysis justified changing only the charges of the deprotonated oxygen, the silicon atom to which it is attached, and that silicon atom's three other coordinated oxygens. Their charge scheme is generally consistent with ours, with similar, but slightly larger, changes to all the atomic charges involved. Our approach is also consistent with that of Lorenz et al. 29 who distributed the negative charge to the bridging oxygen atoms. However, they presented different charge schemes for SiO<sup>-</sup> at different sites (e.g., isolated, vicinal, or geminal), which we have not done here. We note that we have not considered here a charge scheme for deprotonation of a geminal site, which would require further DDEC analysis.

### 3.2.3 Lennard-Jones and Intramolecular Potentials

No new Lennard-Jones parameters were developed for SiO<sup>-</sup> sites, which are described with the same Si and O atom parameters used for the silanols (Table 2).

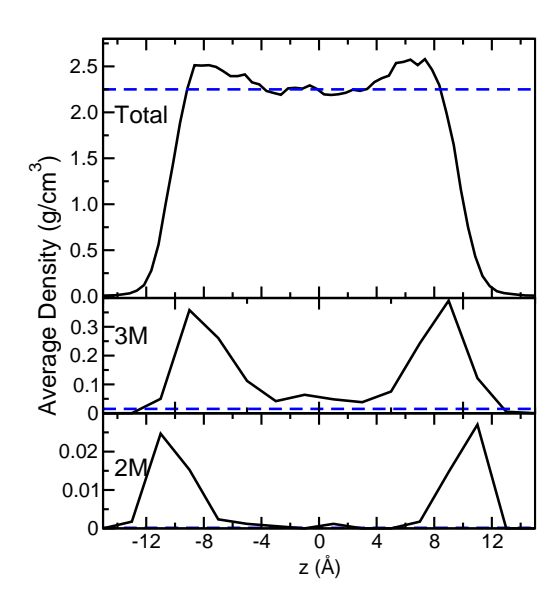


Figure 4: Density profiles of silica-DDEC unfunctionalized amorphous silica slabs (black solid lines), averaged over 100 slab models, plotted as a function of the z-coordinate. Results are shown for all slab atoms (Total) and those in two-membered (2M) and three-membered (3M) rings. Bulk amorphous silica values (blue dashed lines) are shown for comparison.

However, the VASP optimizations of negatively charged amorphous slab models with hydrated sodium ions, produced an intramolecular Si-O<sup>-</sup> bond distance of 1.57 Å. Hence we use this value as the equilibrium bond distance for the harmonic intramolecular Si-O<sup>-</sup> bond stretching potential, while keeping the harmonic constant the same as for the silanol Si-O stretch (though we typically constrain this bond distance). Again, we note that we often fix the Si-O<sup>-</sup> bond length in simulations and the force constants, while reasonable, may need further optimization for studies where a quantitative description of the silanol or Si-O<sup>-</sup> vibrations is desired.

# 4 Validation of the Force Field

In this Section, the results obtained by analyzing amorphous silica, and to a lesser extent crystalline silica, models generated using the silica-DDEC force field are discussed. The

aim is to validate the force field in terms of the structural properties it predicts for the bulk and slab silica structures including density, coordination defects, and ring distributions. Silicawater interfacial properties are examined in the context of refining Lennard-Jones parameters; a detailed examination of silica-liquid interfacial properties will be the focus of a subsequent study.

# 4.1 Predicted amorphous silica structure

Bulk density is a key structural property predicted by a silica force field. The density obtained for bulk amorphous silica models with the silica-DDEC force field is  $2.25 \text{ g/cm}^3$ ; this result is obtained by averaging over 100 individual models created by the melt-quench procedure described in Sec. 2.2. This is consistent with the measured experimental density of  $2.2 \text{ g/cm}^3$  for amorphous  $\text{SiO}_2$ .<sup>74</sup> On the other hand, this result is expected as the density was a key factor in the selection of the Lennard-Jones parameters.

The density profiles of amorphous silica slab models were not involved in the force field parameterization and these results are shown in Fig. 4. There, the total mass density profiles are plotted as a function of the position along the z-coordinate. The average density of bulk amorphous silica are also shown for comparison. In the slab interior, the average density is  $\sim 2.25~{\rm g/cm^3}$ , matching the value for the bulk silica models. In the silica slabs, the density increases near the surface and this is accompanied by a greater population of strained (two- and three-membered) rings (see below). The same behavior has been observed in models based on the BKS  $^{41,75}$  and other force fields.  $^{76}$ 

Bond distances and angles are accessible from experiment <sup>70–73</sup> as well as from the present DFT calculations, both of which, however, only provide average values. The models obtained with the silica-DDEC and other force fields can be analyzed to determine the full normalized probability distribution of Si-O bond distances and Si-O-Si and O-Si-O bond angles. These are shown in Fig. 5. Most of the force

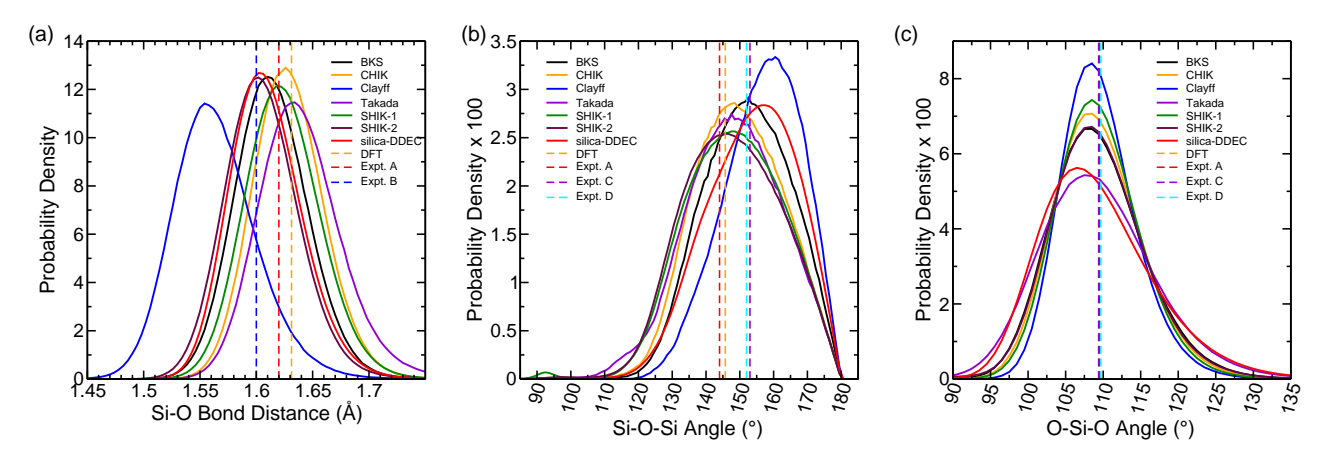


Figure 5: Structural properties of the silica-DDEC bulk amorphous silica models generated with different force fields. Results are shown for the normalized probability distribution of the (a) Si-O bond distance, (b) Si-O-Si angle, and (c) O-Si-O angle. For comparison, average values from the VASP optimizations performed here and experiments (Expt. A = Ref. 70, Expt. B = Ref. 71, Expt. C = Ref. 72, Expt. D = Ref. 73) are shown.

fields yield average values that are in reasonable agreement with experiment, distinguishable from each other by relatively small differences in the peak positions and widths. (An exception is Clayff, which yields Si-O bond distances that are too short and Si-O-Si angles that are too large.) As such, these data represent a check that a force field is reasonable, but do not provide any clear evidence for the superiority of a particular force field. Silica-DDEC gives an average value of the Si-O bond distance of 1.61 Å compared to 1.60 and 1.62 Å from experiment, 70,71 an average Si-O-Si angle of 153.2° compared to measured values of  $144^{\circ}$ ,  $^{70,71}$   $152^{\circ}$ ,  $^{73}$  and  $153^{\circ}$ ,  $^{72}$  and an average O-Si-O angle of 109.3° consistent with measurements of  $109.4 - 109.7^{\circ}$ .  $^{70,72,73}$  At the same time, the silica-DDEC bond and angle distributions do differ, in the details, from some of the other force fields considered, e.g., by having an Si-O-Si angle distribution peaked at larger angles and a broader O-Si-O angle distribution.

# 4.2 Amorphous silica coordination defects

A key issue in classical force field descriptions of silica is the population of coordination defects. For example, while experiments indicate that silica has no five-coordinate silicon atoms, <sup>77–79</sup> many models give significant numbers of such

coordination defects.<sup>39,41</sup> We have thus calculated the percentage of atoms that appear with different coordination defect states; an Si and O atom pair are considered to be coordinated when  $r_{Si-O} \leq 2.2$  Å, a value based on the interatomic radial distribution function.<sup>70</sup>

The percentage of three-, four-, and fivecoordinate silicon atoms as well as one-, twoand three- coordinate oxygen atoms in the silica-DDEC amorphous silica models are given in Table S2. The results are averaged over 100 different realizations of the structure in each case. Results obtained from amorphous silica models generated with a number of common silica force fields in the literature are shown for comparison (averaged over 20 structures for each case). The results show that fourcoordinate silicon is the dominant species, reflecting the tetrahedral arrangement of oxygens around a silicon atom as the most energetically favored arrangement. However, there are small populations of three-coordinate and fivecoordinate Si atoms present.

Compared to bulk amorphous silica, functionalized amorphous silica slabs have more five-coordinate Si defects, however as a percentage it is still low. On average, bulk amorphous silica does not have one-coordinate oxygen defects, but they do appear at surfaces. After our functionalization procedure only 0.1% of oxygen atoms are one-coordinate. The

silica-DDEC force field yields slightly more Si coordination defects than some of the other force fields – several force fields vield 99.9% (99.6-99.8%) four-coordinate Si in bulk amorphous silica (slabs). The difference with the silica-DDEC results are relatively small, however, with 99.8% (99.5%) four-coordinate silicon atoms in the bulk (slabs). On the other hand, silica-DDEC produces fewer O atom coordination defects, giving the smallest percentage of one- and three-coordinate O atoms in both the bulk and slab amorphous silica models. Taken as a whole, these coordination defect data, like the geometric properties discussed above, serve primarily to demonstrate that silica-DDEC provides a credible description of amorphous silica structure (rather than any superiority over existing force fields).

### 4.3 Ring size distribution

The distribution of rings in silica provides information about the strain in the local coordination structure of the atoms. To explore the appearance of strained rings within the silica-DDEC description we calculated the population of rings in the bulk amorphous silica models and the ring density as a function of position in the unfunctionalized slab models. As is customary, we denote the rings by the number of Si atoms. A ring is defined as a closed loop of SiO bonds with a bond defined by  $r_{Si-O} \leq 2.2 \text{ Å}$ , based on the radial distribution function. We note that the connectivity of silicon atoms in silica can be indirectly measured in nuclear magnetic resonance<sup>80</sup> and Raman spectroscopy<sup>81,82</sup> experiments, but we are unaware of any measurement of the ring statistics.

The distribution of ring sizes is shown in Fig. 6a for both bulk and slab silica-DDEC amorphous silica models (100 realizations of each). In both bulk and slab geometries, sixmembered rings are the most common, followed by seven- and five-membered rings. The populations of the remaining (smaller) rings then decline in decreasing order of size.

As has been observed in previous computational studies, <sup>39,41,76,83</sup> there are increased fractions of strained (2M and 3M) rings in the slabs

compared to the bulk. Indeed, in the bulk models, the percentage of two-membered rings is essentially negligible (0.09%). This reflects the fact that the strained rings occur almost exclusively at the silica interface, which can be seen in the density profiles of atoms involved in two- and three-membered rings shown in Fig. 4. The presence of these strained rings is also evident from the observation of minor peaks at small angles ( $\sim 80 - 90^{\circ}$ ) in the Si-O-Si and O-Si-O angle distributions shown in Figure 5. These strained rings are likely reaction sites on the surface that can react with water to form silanols, making them particularly significant when studying silica-water interfaces. <sup>76</sup> This is the motivation for the ad hoc functionalization procedure used here and described in Sec. 2.2, which is based on hydrolysis of water across these strained rings.

The silica-DDEC ring distribution is compared, for unfunctionalized slab models, to those for several other force fields in Fig. 6b. All of the force fields yield qualitatively similar results with six-membered rings being most prevalent. Some quantitative differences are observed, e.g., Clayff yields fewer strained two-and three-membered rings, while SHIK-1 gives more of these rings.

#### 4.4 Silica-water interactions

Finally, we have carried out a preliminary investigation of a 3 nm water-filled slit pore constructed from a silica-DDEC derived functionalized amorphous silica slab as described in Sec. 2.2. A key aim is to understand whether the silica-DDEC Lennard-Jones parameters, which are designed to reproduce the amorphous silica structural properties, need to be modified to describe the interactions with a liquid at the silica interface. As we now discuss, the answer is yes, but appropriate modifications are straightforward.

The MD simulations of the slit pore were used to calculate the probability distribution for different interatomic distances involving the water H and O atoms and atoms in the silica slab. The SPC/E model<sup>55</sup> was used to describe the water molecules and the silica atoms were al-

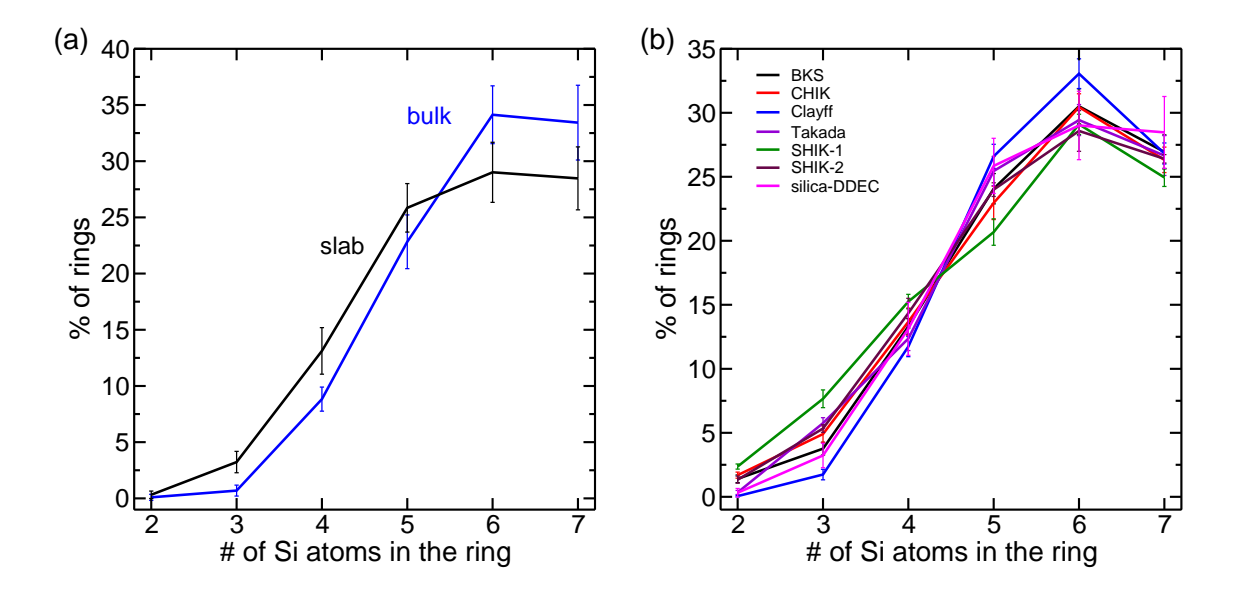


Figure 6: Ring distributions for (a) amorphous bulk silica (blue line) and unfunctionalized silica slabs (black line) from the silica-DDEC force field, and (b) unfunctionalized silica slabs generated with different force fields. "Error" bars indicate a standard deviation over 100 models for silica-DDEC (20 models for all other FFs), providing an insight into the heterogeneity of the systems.

lowed to move as described in Sec. 2.2. We first used the "intra-silica" Lennard-Jones parameters obtained, as described above, based on reproducing the silica structural properties. The parameters are given in Table 2 and combined with those for SPC/E water using Lorentz-Berthelot mixing rules. These results are shown as black lines in Fig. 7; the plots show the normalized probability distribution of each water atom type  $(H_W \text{ or } O_W)$  to the closest silica atom of each type for all the water molecules in the simulation. When the distributions are compared to the average distances found in abinitio MD studies in the literature, <sup>12,27</sup> we find that water-surface distances are reduced when the intra-silica parameters are used directly. In particular, the first peak positions are shifted to smaller distances for the distribution of water H and O atoms relative to bridging O atoms in silica. The same is true of the water O-silica Si distribution, which also exhibits a small peak at distances less than 2 Å due to a water closely approaching a single silanol Si. This indicates that the silica-DDEC Lennard-Jones parameters for these atoms in silica should be modified to properly describe the interactions with a liquid. One approach to a solution is apparent in the comparatively good agreement with

the *ab initio* MD distances for the silanol sites, also shown in Fig. 7. Recall that the silanol O atoms have Lennard-Jones parameters significantly larger than the bridging O atoms (Table 2), with  $\sigma$  values closer to that of water models.

This suggests that the interaction of the bridging O atoms with water would be better described with Lennard-Jones parameters like those of the silanol oxygens. Thus, we repeated the simulations with modified Lennard-Jones parameters for all silica oxygen atoms, only in their interactions with the external water molecules. These silica-water parameters are taken to be the same as for the silanol oxygen atoms and are used with Lorentz-Berthelot mixing rules, i.e.,  $\sigma_{O-O_w} = \sigma_{O(H)-O_w}$  $[\sigma_{O(H)} + \sigma_{O_w}]/2$  and  $\epsilon_{O-O_w} = \epsilon_{O(H)-O_w} =$  $\sqrt{\epsilon_{O(H)} \epsilon_{O_w}}$ . The results from simulations with these modified Lennard-Jones interactions are shown as red lines in Fig. 7. This simple change dramatically improves the agreement with the ab initio MD results 12,27 for the peak positions in the distributions of the water atoms with the bridging oxygen sites, with no adverse effects on the silanol-water distances. The distributions for deprotonated site with water are shown in Fig. S8 of the Supporting Information.

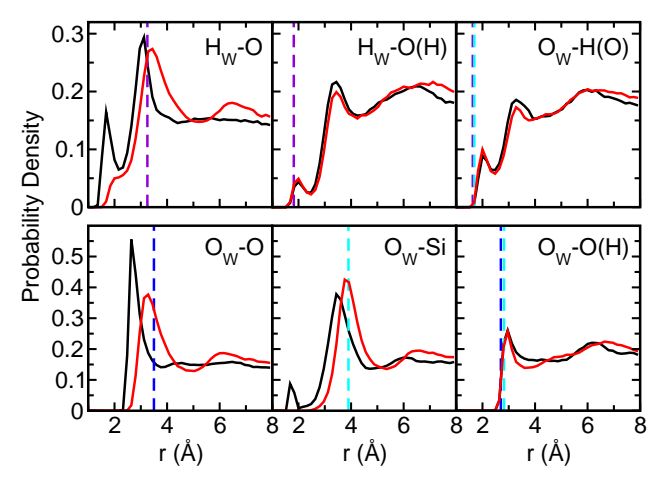


Figure 7: Probability distributions of the distance of water atoms to the nearest silica atom. Here, a subscript w indicates an atom in a water molecule while O(H) and H(O) indicate a silanol oxygen and hydrogen, respectively, and O denotes a bridging oxygen in silica. sults are shown for SPC/E water using the "intra-silica" parameters (black lines) and with the modified "silica-water" Lennard-Jones pair parameters (red lines); both parameter sets are given in Table 2 and used with Lorentz-Berthelot mixing rules. The dashed lines represent DFT results from Ref. 27 (blue) and Ref. 12 (purple) for silica slabs. The dashed cyan lines show DFT results from Ref. 27 for an orthosilicic acid cluster.

The second component of the adjustments is in the Si atom interactions with water to eliminate the small peak in the  $O_w$ -Si distribution at small distances. This is accomplished by increasing  $\sigma_{Si}$  to 3.0 Å and  $\epsilon_{Si}$  to 0.01 kcal/mol. In addition to preventing artificially close approaches of water molecules to the silica atoms, it gives  $O_w$ -Si distances in good agreement with ab initio MD. <sup>12,27</sup>

It is possible that further adjustment of the Lennard-Jones parameters will be required to accurately describe the interfacial silica interactions with other liquids. This will require additional study. However, the silica-DDEC force field is able to accurately describe these water-silica structural properties with this modification of the bridging oxygen parameters.

### 5 Conclusions

By using electronic structure-derived charges and systematic exploration of the non-bonding interaction potential, we have developed a novel force field for amorphous and crystalline silica. Unlike many other silica force fields in the literature, atomic charges were derived using periodic rather than cluster models, and they reproduce the electrostatic potential in the bulk structures and at interfaces. We developed a charge scheme for both neutral and charged surfaces and successfully modeled amorphous and crystalline bulk as well as surfaces using it. Importantly, neutral and charged silica surfaces can be described with full flexibility, unlike other silica studies in which some surface atoms are fixed.

We investigated structural properties of silica to validate the force field. The density of bulk silica is comparable to the experimental density and the generated bulk as well as slab systems have a very low percentage of coordination defects. We also examined the distribution of rings in the silica structure and found that silica surfaces have more strained rings compared to bulk and two-membered rings are found almost exclusively at the slab interface, which is comparable to experimental studies.

A key advantage of the silica-DDEC force field is that it is parameterized for both bulk and slab silica models. In addition, it is transferable to silica-water interfaces, with a simple adjustment to the silica-water Lennard-Jones parameters. It is reasonable to expect that this force field will also be directly applicable to other fluids interacting with silica, which will be explored in future studies. Thus, it should be of use to researchers interested in these interfaces that are both ubiquitous and technologically important.

### Acknowledgments

The authors thank Dr. Anastasia G. Ilgen and Kevin Leung for many useful discussions. The force field development work was supported by the US Department of Energy, Office of Sci-

ence, Office of Basic Energy Sciences, Chemical Sciences, Geosciences and Biosciences Division under Field Work Proposal No. 21-015452. The results for other force fields was supported by the US Department of Energy, Office of Basic Energy Sciences, Computational Chemical Sciences grant No. DE-SC-0019488. This article has been authored by an employee of National Technology & Engineering Solutions of Sandia, LLC under Contract No. DE-NA0003525 with the U.S. Department of Energy (DOE). The employee owns all right, title and interest in and to the article and is solely responsible for its contents. The United States Government retains and the publisher, by accepting the article for publication, acknowledges that the United States Government retains a non-exclusive, paid-up, irrevocable, worldwide license to publish or reproduce the published form of this article or allow others to do so, for United States Government pur-The DOE will provide public access poses. to these results of federally sponsored research in accordance with the DOE Public Access Plan https://www.energy.gov/downloads/doepublic-access-plan. The views and opinions expressed herein do not necessarily state or reflect those of the United States Government, any agency thereof, or any of their contractors. The calculations were performed at the University of Kansas Center for Research Computing (CRC), including the BigJay cluster resource funded through NSF Grant No. MRI-2117449.

### **Supporting Information**

System parameters, DDEC charge distributions, melt-quench density profiles, intramolecular potential parameters, amorphous silica structure characterization, details of the other force fields used, and water structure near deprotonated sites.

### References

(1) Wang, Y. Nanogeochemistry: Nanostructures, emergent properties and their con-

- trol on geochemical reactions and mass transfers. *Chem. Geol.* **2014**, *378-379*, 1–23.
- (2) Götze, J.; Möckel, R.; Pan, Y. Mineralogy, geochemistry and genesis of agate A review. *Minerals* **2020**, *10*, 1037.
- (3) Belonoshko, A. The thermodynamics of the aqueous carbon dioxide fluid within thin pores. *Geochim. Cosmochim. Acta* **1989**, *53*, 2581–2590.
- (4) Rimsza, J. M.; Jones, R. E.; Criscenti, L. J. Chemical effects on subcritical fracture in silica from molecular dynamics simulations. *J. Geophys. Res.* **2018**, *123*, 9341–9354.
- (5) Zhao, H.; Nagy, K. L.; Waples, J. S.; Vance, G. F. Surfactant-templated mesoporous silicate materials as sorbents for organic pollutants in water. *Environ. Sci. Technol.* 2000, 34, 4822–4827.
- (6) Sang, S. H.; Shorted, M. R.; Young, E. S. Real-time dynamics of single-DNA molecules undergoing adsorption and desorption at liquid-solid interfaces. *Anal. Chem.* 2001, 73, 1091–1099.
- (7) Lochmuller, C. H.; Wenzel, T. J. Spectroscopic studies of pyrene at silica interfaces. J. Phys. Chem. 1990, 94, 4230–4235.
- (8) Leung, K.; Nielsen, I. M. B.; Criscenti, L. J. Elucidating the bimodal acid-base behavior of the water-silica interface from first principles. *J. Am. Chem. Soc.* **2009**, *131*, 18358–18365.
- (9) Skelton, A. A.; Wesolowski, D. J.; Cummings, P. T. Investigating the quartz (1010)/water interface using classical and ab initio molecular dynamics. Langmuir **2011**, 27, 8700–8709.
- (10) Gaigeot, M.-P.; Sprik, M.; Sulpizi, M. Oxide/water interfaces: How the surface chemistry modifies interfacial water properties. J. Phys.-Condens. Mat. 2012, 24, 124106.

- (11) Sulpizi, M.; Gaigeot, M.-P.; Sprik, M. The silica—water interface: How the silanols determine the surface acidity and modulate the water properties. *J. Chem. Theor. Comp.* **2012**, *8*, 1037–1047.
- (12) Cimas, A.; Tielens, F.; Sulpizi, M.; Gaigeot, M.-P.; Costa, D. The amorphous silica-liquid water interface studied by *ab initio* molecular dynamics (AIMD): Local organization in global disorder. *J. Phys.-Condens. Mat.* **2014**, *26*, 244106.
- (13) Pfeiffer-Laplaud, M.; Costa, D.; Tielens, F.; Gaigeot, M.-P.; Sulpizi, M. Bimodal acidity at the amorphous silica/water interface. *J. Phys. Chem. C* **2015**, *119*, 27354–27362.
- (14) Pfeiffer-Laplaud, M.; Gaigeot, M.-P.; Sulpizi, M.  $pK_a$  at quartz/electrolyte interfaces. J. Phys. Chem. Lett. **2016**, 7, 3229–3234.
- (15) Parashar, S.; Lesnicki, D.; Sulpizi, M. Increased acid dissociation at the quartz/water interface. J. Phys. Chem. Lett. **2018**, *9*, 2186–2189.
- (16) Gierada, M.; De Proft, F.; Sulpizi, M.; Tielens, F. Understanding the acidic properties of the amorphous hydroxylated silica surface. J. Phys. Chem. C 2019, 123, 17343–17352.
- (17) Mahadevan, T. S.; Garofalini, S. H. Dissociative chemisorption of water onto silica surfaces and formation of hydronium ions. J. Phys. Chem. B 2008, 112, 1507–1515.
- (18) Lockwood, G. K.; Garofalini, S. H. Proton dynamics at the water-silica interface via dissociative molecular dynamics. J. Phys. Chem. C 2014, 118, 29750–29759.
- (19) van Duin, A.; Strachan, A.; Stewman, S.; Zhang, Q.; Xu, X.; Goddard, W. ReaxFF<sub>SiO</sub> reactive force field for silicon and silicon oxide systems. J. Phys. Chem. A 2003, 107, 3803–3811.

- (20) Kulkarni, A. D.; Truhlar, D. G.; Goverapet Srinivasan, S.; van Duin, A. C. T.; Norman, P.; Schwartzentruber, T. E. Oxygen interactions with silica surfaces: Coupled cluster and density functional investigation and the development of a new ReaxFF potential. J. Phys. Chem. C 2013, 117, 258–269.
- (21) Yeon, J.; van Duin, A. C. T. ReaxFF molecular dynamics simulations of hydroxylation kinetics for amorphous and nano-silica structure, and its relations with atomic strain energy. J. Phys. Chem. C 2016, 120, 305–317.
- (22) Bródka, A.; Zerda, T. W. Properties of liquid acetone in silica pores: Molecular dynamics simulation. J. Chem. Phys. 1996, 104, 6319–6326.
- (23) Cygan, R. T.; Liang, J.-J.; Kalinichev, A. G. Molecular models of hydroxide, oxyhydroxide, and clay phases and the development of a general force field. J. Phys. Chem. B 2004, 108, 1255–1266.
- (24) Gulmen, T. S.; Thompson, W. H. Model silica pores with controllable surface chemistry for molecular dynamics simulations. Dynamics in Small Confining Systems VIII, edited by JT Fourkas, P. Levitz, R. Overney, M. Urbakh (Mater. Res. Soc. Symp. Proc. 899E, Warrendale, PA, 2005)
- (25) Gulmen, T. S.; Thompson, W. H. Testing a two-state model of nanoconfined liquids: conformational equilibrium of ethylene glycol in amorphous silica pores. Langmuir 2006, 22, 10919–10923.
- (26) Hassanali, A. A.; Singer, S. J. Model for the water-amorphous silica interface: The undissociated surface. *J. Phys. Chem. B* **2007**, *111*, 11181–11193.
- (27) Hassanali, A. A.; Zhang, H.; Knight, C.; Shin, Y. K.; Singer, S. J. The dissociated

- amorphous silica surface: Model development and evaluation. J. Chem. Theory Comput. **2010**, 6, 3456–3471.
- (28) Pedone, A.; Malavasi, G.; Menziani, M. C.; Segre, U.; Musso, F.; Corno, M.; Civalleri, B.; Ugliengo, P. FFSiOH: A new force field for silica polymorphs and their hydroxylated surfaces based on periodic B3LYP calculations. *Chem. Mater.* **2008**, *20*, 2522–2531.
- (29) Lorenz, C. D.; Crozier, P. S.; Anderson, J. A.; Travesset, A. Molecular dynamics of ionic transport and electrokinetic effects in realistic silica channels. *J. Phys. Chem. C* **2008**, *112*, 10222–10232.
- (30) Butenuth, A.; Moras, G.; Schneider, J.; Koleini, M.; Köppen, S.; Meißner, R.; Wright, L. B.; Walsh, T. R.; Ciacchi, L. C. Ab initio derived force-field parameters for molecular dynamics simulations of deprotonated amorphous-SiO<sub>2</sub>/water interfaces. Phys. Status Solidi B **2012**, 249, 292–305.
- (31) Emami, F. S.; Puddu, V.; Berry, R. J.; Varshney, V.; Patwardhan, S. V.; Perry, C. C.; Heinz, H. Force field and a surface model database for silica to simulate interfacial properties in atomic resolution. *Chem. Mater.* **2014**, *26*, 2647–2658.
- (32) Manz, T. A.; Sholl, D. S. Improved atoms-in-molecule charge partitioning functional for simultaneously reproducing the electrostatic potential and chemical states in periodic and nonperiodic materials. *J. Chem. Theory Comput.* **2012**, *8*, 2844–2867.
- (33) Limas, N. G.; Manz, T. A. Introducing DDEC6 atomic population analysis: part 4. Efficient parallel computation of net atomic charges, atomic spin moments, bond orders, and more. RSC Adv. 2018, 8, 2678–2707.
- (34) Manz, T. A.; Sholl, D. S. Chemically meaningful atomic charges that reproduce

- the electrostatic potential in periodic and nonperiodic materials. *J. Chem. Theor. Comput.* **2010**, *6*, 2455–2468.
- (35) van Beest, B. W. H.; Kramer, G. J.; van Santen, R. A. Force fields for silicas and aluminophosphates based on *ab initio* calculations. *Phys. Rev. Lett.* **1990**, *64*, 1955–1958.
- (36) Dubbeldam, D.; Walton, K. S.; Ellis, D. E.; Snurr, R. Q. Exceptional negative thermal expansion in isoreticular metal-organic frameworks. *Angew. Chem. Int. Ed.* **2007**, *46*, 4496–4499.
- (37) Cruz-Chu, E. R.; Aksimentiev, A.; Schulten, K. Water-silica force field for simulating nanodevices. *J. Phys. Chem. B* **2006**, 110, 21497–21508.
- (38) Sundararaman, S.; Ching, W.-Y.; Huang, L. Mechanical properties of silica glass predicted by a pair-wise potential in molecular dynamics simulations. J. Non-Cryst. Solids 2016, 445-446, 102–109.
- (39) Vollmayr, K.; Kob, W.; Binder, K. Cooling-rate effects in amorphous silica: A computer-simulation study. *Phys. Rev. B* **1996**, *54*, 15808–15827.
- (40) Afify, N.; Mountjoy, G.; Haworth, R. Selecting reliable interatomic potentials for classical molecular dynamics simulations of glasses: The case of amorphous SiO<sub>2</sub>. Comp. Mater. Sci. 2017, 128, 75–80.
- (41) Wimalasiri, P. N.; Nguyen, N. P.; Senanayake, H. S.; Laird, B. B.; Thompson, W. H. Amorphous silica slab models with variable surface roughness and silanol density for use in simulations of dynamics and catalysis. *J. Phys. Chem. C* **2021**, 125, 23418–23434.
- (42) Fang, H. J.; Kamakoti, P.; Zang, J.; Cundy, S.; Paur, C.; Ravikovitch, P. I.; Sholl, D. S. Prediction of CO<sub>2</sub> adsorption properties in zeolites using force fields derived from periodic dispersion-corrected

- DFT calculations. *J. Phys. Chem. C* **2012**, *116*, 10692–10701.
- (43) Haldoupis, E.; Borycz, J.; Shi, H.; Vogiatzis, K. D.; Bai, P.; Queen, W. L.; Gagliardi, L.; Siepmann, J. I. Ab initio derived force fields for predicting CO<sub>2</sub> adsorption and accessibility of metal sites in the metal-organic frameworks M-MOF-74 (M = Mn, Co, Ni, Cu). J. Phys. Chem. C 2015, 119, 16058–16071.
- (44) Jorge, M.; Milne, A. W.; Barrera, M. C.; Gomes, J. R. B. New force-field for organosilicon molecules in the liquid phase. *ACS Phys. Chem. Au* **2021**, *1*, 54–69.
- (45) Findley, J. M.; Boulfelfel, S. E.; Η. J.; G.; Fang, Muraro, Ravikovitch, P. I.; Sholl, D. S. transferable force field for predicting adsorption and diffusion of hydrocarbons and small molecules in silica zeolites with coupled-cluster accuracy. J. Phys. Chem. C **2021**, 125, 8418–8429.
- (46) Kresse, G.; Hafner, J. Ab initio molecular dynamics for liquid metals. Phys. Rev. B 1993, 47, 558–561.
- (47) Kresse, G.; Furthmüller, J. Efficiency of ab-initio total energy calculations for metals and semiconductors using a plane-wave basis set. Comput. Mater. Sci. 1996, 6, 15–50.
- (48) Kresse, G.; Furthmüller, J. Efficient iterative schemes for *ab initio* total-energy calculations using a plane-wave basis set. *Phys. Rev. B* **1996**, *54*, 11169–11186.
- (49) Thompson, A. P.; Aktulga, H. M.; Berger, R.; Bolintineanu, D. S.; Brown, W. M.; Crozier, P. S.; in 't Veld, P. J.; Kohlmeyer, A.; Moore, S. G.; Nguyen, T. D. et al. LAMMPS a flexible simulation tool for particle-based materials modeling at the atomic, meso, and continuum scales. Comput. Phys. Commun. 2022, 271, 108171.

- (50) Berendsen, H. J. C.; Postma, J. P. M.; van Gunsteren, W. F.; DiNola, A.; Haak, J. R. Molecular dynamics with coupling to an external bath. J. Chem. Phys. 1984, 81, 3684–3690.
- (51) Cygan, R. T.; Liang, J.-J.; Kalinichev, A. G. Molecular models of hydroxide, oxyhydroxide, and clay phases and the development of a general force field. J. Phys. Chem. B 2004, 108, 1255–1266.
- (52) Takada, A.; Richet, P.; Catlow, C. R. A.; Price, G. D. Molecular dynamics simulations of vitreous silica structures. *J. Non-Cryst. Solids* **2004**, *345–346*, 224–229.
- (53) Carré, A.; Horbach, J.; Ispas, S.; Kob, W. New fitting scheme to obtain effective potential from Car-Parrinello molecular dynamics simulations: Application to silica. *Europhys. Lett.* **2008**, *82*, 17001.
- (54) Sundararaman, S.; Huang, L.; Ispas, S.; Kob, W. New optimization scheme to obtain interaction potentials for oxide glasses. J. Chem. Phys. 2018, 148, 194504.
- (55) Berendsen, H. J. C.; Grigera, J. R.; Straatsma, T. P. The missing term in effective pair potentials. *J. Phys. Chem.* **1987**, *91*, 6269–6271.
- (56) Ryckaert, J. P.; Ciccotti, G.; Berendsen, H. J. Numerical integration of the Cartesian equations of motion of a system with constraints: molecular dynamics of n-alkanes. J. Comput. Phys. 1977, 23, 327–341.
- (57) Humphrey, W.; Dalke, A.; Schulten, K. VMD Visual Molecular Dynamics. *J. Mol. Graphics* **1996**, *14*, 33–38.
- (58) Barth, T. F. W. The cristobalite structures: I. High-cristobalite. Am. J. Sci. **1932**, 23, 350–356.

- (59) Joseph, S.; Aluru, N. R. Hierarchical multiscale simulation of electrokinetic transport in silica nanochannels at the point of zero charge. *Langmuir* **2006**, *22*, 9041–9051.
- (60) Morales, C. M.; Thompson, W. H. Simulations of infrared spectra of nanoconfined liquids: Acetonitrile confined in nanoscale, hydrophilic silica pores. *J. Phys. Chem. A* **2009**, *113*, 1922–1933.
- (61) Norton, C. D.; Thompson, W. H. On the diffusion of acetonitrile in nanoscale amorphous silica pores. understanding anisotropy and the effects of hydrogen bonding. J. Phys. Chem. C 2013, 117, 19107–19114.
- (62) Burris, P. C.; Laage, D.; Thompson, W. H. Simulations of the infrared, Raman, and 2D-IR photon echo spectra of water in nanoscale silica pores. J. Chem. Phys. 2016, 144, 194709.
- (63) Senanayake, H. S.; Greathouse, J. A.; Ilgen, A. G.; Thompson, W. H. Simulations of the IR and Raman spectra of water confined in amorphous silica slit pores. *J. Chem. Phys.* **2021**, *154*, 104503.
- (64) Tangney, P.; Scandolo, S. An ab initio parametrized interatomic force field for silica. J. Chem. Phys. 2002, 117, 8898–8904.
- (65) Hill, J.-R.; Sauer, J. Molecular mechanics potential for silica and zeolite catalysts based on *ab initio* calculations. 1. Dense and microporous silica. *J. Phys. Chem.* **1994**, *98*, 1238–1244.
- (66) Hill, J.-R.; Sauer, J. Molecular mechanics potential for silica and zeolite catalysts based on *ab initio* calculations. 2. Aluminosilicates. *J. Phys. Chem.* **1995**, *99*, 9536–9550.
- (67) Vashishta, P.; Kalia, R. K.; Rino, J. P.; Ebbsjö, I. Interaction potential for SiO<sub>2</sub>: A molecular-dynamics study of structural correlations. *Phys. Rev. B* **1990**, 41, 12197–12209.

- (68) Abascal, J. L. F.; Vega, C. A general purpose model for the condensed phases of water: TIP4P/2005. *J. Chem. Phys.* **2005**, *123*, 234505.
- (69) Kroutil, O.; Chval, Z.; Skelton, A. A.; Předota, M. Computer simulations of quartz (101)-water interface over a range of pH values. J. Phys. Chem. C 2015, 119, 9274–9286.
- (70) Mozzi, R.; Warren, B. The structure of vitreous silica. *J. Appl. Crystallogr.* **1969**, 2, 164–172.
- (71) Khouchaf, L.; Boulahya, K.; Das, P. P.; Nicolopoulos, S.; Kis, V. K.; Lábár, J. L. Study of the microstructure of amorphous silica nanostructures using high-resolution electron microscopy, electron energy loss spectroscopy, X-ray powder diffraction, and electron pair distribution function. *Materials* **2020**, *13*, 4393.
- (72) Da Silva, J. R. G.; Pinatti, D. G.; Anderson, C. E.; Rudee, M. L. A refinement of the structure of vitreous silica. *Philos. Mag.* 1975, 31, 713–717.
- (73) Coombs, P. G.; De Natale, J. F.; Hood, P. J.; McElfresh, E. K.; Wortman, R. S.; Schackelford, J. F. The nature of the Si-O-Si bond angle distribution in vitreous silica. *Philos. Mag.* 1985, 51, L39-L42.
- (74) Mazurin, O. V.; Streltsina, M. V.; Shvaiko-Shvaikovskaya, T. P. *Handbook of Glass Data, Part A: Silica Glass and Binary Silicate Glasses*; Elsevier: Amsterdam, 1983.
- (75) Zhang, Z.; Kob, W.; Ispas, S. First-principles study of the surface of silica and sodium silicate glasses. *Phys. Rev. B* **2021**, *103*, 184201.
- (76) Roder, A.; Kob, W.; Binder, K. Structure and dynamics of amorphous silica surfaces. *J. Chem. Phys.* **2001**, *114*, 7602–7614.

- (77) Zeidler, A.; Wezka, K.; Rowlands, R. F.; Whittaker, D. A.; Salmon, P. S.; Polidori, A.; Drewitt, J. W.; Klotz, S.; Fischer, H. E.; Wilding, M. C. et al. Highpressure transformation of SiO<sub>2</sub> glass from a tetrahedral to an octahedral network: A joint approach using neutron diffraction and molecular dynamics. *Phys. Rev. Lett.* **2014**, *113*, 1–5.
- (78) Benmore, C. J.; Soignard, E.; Amin, S. A.; Guthrie, M.; Shastri, S. D.; Lee, P. L.; Yarger, J. L. Structural and topological changes in silica glass at pressure. *Phys. Rev. B* **2010**, *81*, 054105.
- (79) Salmon, P. S.; Zeidler, A. Networks under pressure: The development of *in situ* high-pressure neutron diffraction for glassy and liquid materials. *J. Phys. Condens. Matter* **2015**, *27*, 133201.
- (80) Maekawa, H.; Yokokawa, T. Effects of temperature on silicate melt structure: A high temperature <sup>29</sup>Si NMR study of Na<sub>2</sub>Si<sub>2</sub>O<sub>5</sub>. Geochem. J. **1997**, 61, 2569–2575.
- (81) Galeener, F. Planar rings in glasses. Solid State Commun. 1982, 44, 1037–1040.
- (82) Galeener, F. L. Planar rings in vitreous silica. J. Non-Cryst. Solids 1982, 49, 53–62.
- (83) Levine, S.; Garofalini, S. A structural analysis of the vitreous silica surface via a molecular dynamics computer simulation. J. Chem. Phys. 1987, 86, 2997–3002.

### TOC Graphic

